Труды Карельского научного центра РАН. 2025. № 2. С. 111–125
Transactions of the Karelian Research Centre RAS. 2025. No. 2. P. 111–125
DOI: 10.17076/lim2060

УДК 551.46.09 : 528.852 : 581.526.325.3 : 551.515.2

SATELLITE DATA ANALYSIS OF THE PHYTOPLANKTON COMMUNITY STRUCTURE VARIATIONS ON DIFFERENT TIME SCALES IN THE SOUTH CHINA SEA

E. A. Morozov[1,2]*, H. Ye[3], D. Tang[2,3], D. V. Pozdnyakov[4], Y. Liu[2,3]

*[1] Marine Hydrophysical Institute, Russian Academy of Sciences (2 Kapitanskaya St., 299011 Sevastopol, Russia), * frisman@list.ru*
[2] Southern Marine Science and Engineering Guangdong Laboratory (Guangzhou) (1119 Haibin Road, Information Technology Park, Nansha Street, Nansha District, 511458 Guangzhou, China)
[3] State Key Laboratory of Tropical Oceanography, Guangdong Key Laboratory of Ocean Remote Sensing, South China Sea Institute of Oceanology, Chinese Academy of Sciences (164 Xingangxi Rd, Haizhu District, 510301 Guangzhou, Guandong, China)
[4] Nansen International Environmental and Remote Sensing Center (14th Line, 7, Office 49, Vasilievsky Island, 199034 St. Petersburg, Russia)

Here we report on our studies of chlorophyll-a in the South China Sea (SCS) and its structural features based solely on merged satellite ocean color data (Ocean Color Climate Change Initiative – OC-CCI). The SCS is largely oligotrophic, and its primary production predominantly comes from picophytoplankton. Short-term changes in the SCS picophytoplankton community structure driven by typhoon Wind Pump (WP) are studied against the background of long-term (1998–2016) space-borne OC-CCI observation data. Two ocean color data processing algorithms were applied permitting to reveal (a) the SCS total phytoplankton size structure (in terms of its contribution to chlorophyll-a (chl-a) concentration), and (b) the picophytoplankton community structure. The first algorithm is for partitioning the total chl-a in water into micro-, nano-, and picophytoplankton. The second algorithm quantifies the cell abundances of two species of prokaryotic algae – *Prochlorococcus* (Pro) and *Synechococcous* (Syn), and the entire community of eukaryotic picophytoplankton (Peuk) in the SCS. In general, a long-term trend toward an increase in chl-a of all phytoplankton size classes was observed, although the relative share of micro- and nanophytoplankton in the total amount of chl-a was minor, while the share of picophytoplankton was somewhat more pronounced. Within the picophytoplankton size class, the numbers of Syn and Peuk cells also showed a slight upward trend, whereas Pro showed a definite decrease in their numbers. The short-term dynamics caused by the passing typhoons was marked by a strong growth of chl-a along the cyclone's footprint path, with the potential to eventually promote massive phytoplankton blooms. Within the picophytoplankton size fraction, Syn and Peuk cell numbers showed some increase, while Pro cells, which proved to be resistant to poor nutrient conditions, decreased when the typhoon wind pump effect provided nutrients. The typhoon WP temporal effect on phytoplankton community structure was shown to last not more than 1 month, but usually 2-3 weeks. Our results indicate that the above two data processing algorithms are instrumental in establishing the phytoplankton community structure status and its dynamics in the SCS.

Keywords: South China Sea; Typhoons; Wind pump; Phytoplankton community structure; Merged ocean color data

For citation: Morozov E. A., Ye H., Tang D., Pozdnyakov D. V., Liu Y. Satellite data analysis of the phytoplankton community structure variations on different time scales in the South China Sea. *Trudy Karel'skogo nauchnogo tsentra RAN = Transactions of the Karelian Research Centre RAS*. 2025. No. 2. P. 111–125. doi: 10.17076/lim2060

Funding. This study was funded by the Foundation of Guangdong Science and Technology Department (2019BT2H594, 2017B030301005), state assignment to the Marine Hydrophysical Institute FNNN-2024-0012, Key Project (41430968, 41876136) of the National Natural Sciences Foundation of China, and Russian Foundation for Basic Research (20-35-70034).

Е. А. Морозов[1,2*], Х. Йе[3], Д. Тан[2,3], Д. В. Поздняков[4], Ю. Лиу[2,3]. ИССЛЕДОВАНИЕ ВРЕМЕННОЙ ИЗМЕНЧИВОСТИ СТРУКТУРЫ ФИТОПЛАНКТОННОГО СООБЩЕСТВА В ЮЖНО-КИТАЙСКОМ МОРЕ ПО СПУТНИКОВЫМ ДАННЫМ НА РАЗЛИЧНЫХ ВРЕМЕННЫХ МАСШТАБАХ

[1] *Морской гидрофизический институт РАН (ул. Капитанская, 2, Севастополь, Россия, 299011), frisman@list.ru*

[2] *Южная морская научно-инженерная лаборатория провинции Гуандун (Гуанчжоу, КНР, 511458)*

[3] *Государственная лаборатория тропической океанографии, Гуандунская лаборатория дистанционного зондирования океана, Институт океанологии Южно-Китайского моря Академии наук Китая (Гуанчжоу, КНР, 510301)*

[4] *Международный центр по окружающей среде и дистанционному зондированию имени Нансена (14-я линия В. О., 7, оф. 49, Санкт-Петербург, Россия, 199034)*

Проведено исследование хлорофилла *a* фитопланктона в Южно-Китайском море и его структурных особенностей, основанных исключительно на объединенных спутниковых данных о цвете океана (Ocean Colour Climate Change Initiative). Южно-Китайское море в значительной степени олиготрофно, и его первичная продукция в основном обеспечивается пикофитопланктоном. Краткосрочные изменения в структуре сообщества пикофитопланктона Южно-Китайского моря, вызванные эффектом ветрового насоса, обусловленного тайфунами, изучаются на основе многолетних (1998–2016 гг.) мультисенсорных спутниковых данных. Применены два алгоритма обработки данных о цвете океана. Первый позволяет выявить общую размерную структуру фитопланктона (с точки зрения его вклада в концентрацию хлорофилла *a* (chl-a)) и разделить общий chl-a в воде на микро-, нано- и пикофитопланктон. Второй алгоритм количественно оценивает численность клеток трех групп пикофитопланктона, а именно: двух видов прокариотических водорослей Prochlorococcus и Synechococcous и всего сообщества эукариотического пикофитопланктона (пикоэукариоты). В целом наблюдалась долгосрочная тенденция к увеличению chl-a всех размерных классов фитопланктона, хотя относительная доля микро- и нанофитопланктона в общем количестве chl-a была незначительной, в то время как доля пикофитопланктона была несколько более выраженной. Внутри размерного класса пикофитопланктона количество клеток Synechococcous и пикоэукариотов также показало небольшую тенденцию к росту, тогда как численность Prochlorococcus снижалась. Краткосрочная изменчивость, вызванная влиянием прохождения тайфунов, характеризуется сильным ростом chl-a вдоль траектории прохождения, что в конечном итоге может способствовать массовому цветению фитопланктона и увеличению вклада более крупного фитопланктона в общую концентрацию chl-a. В составе пикофитопланктона количество клеток Synechococcus и пикоэукариотов показало некоторое увеличение, в то время как число клеток Prochlorococcus, которые адаптированы к олиготрофным условиям отсутствия тайфунов, уменьшалось. Показано, что временное воздействие ветрового насоса, вызванного тайфуном, на фитопланктонное сообщество длится не более 1 месяца, обычно 2–3 недели. Полученные результаты показывают, что два вышеуказанных

алгоритма обработки данных могут играть важную роль в установлении структуры фитопланктонного сообщества и его динамики в Южно-Китайском море.

Ключевые слова: Южно-Китайское море; тайфуны; ветровой насос; структура сообщества фитопланктона; объединенные данные о цвете океана

Для цитирования: Morozov E. A., Ye H., Tang D., Pozdnyakov D. V., Liu Y. Satellite data analysis of the phytoplankton community structure variations on different time scales in the South China Sea. *Trudy Karel'skogo nauchnogo tsentra RAN = Transactions of the Karelian Research Centre RAS*. 2025. No. 2. P. 111–125. doi: 10.17076/lim2060

Финансирование. Финансовое обеспечение исследований осуществлялось в рамках государственного задания Морского гидрофизического института РАН (FNNN-2024-0012), ключевого проекта (41430968, 41876136) Государственного фонда естественных наук Китая, а также Отделением науки и технологии фонда провинции Гуандун (2019BT2H594, 2017B030301005) и Российским фондом фундаментальных исследований (20-35-70034).

Introduction

The concentration of phytoplankton chlorophyll-a (chl-a) is traditionally considered as a valuable parameter shedding light on the ecological state of water bodies and their productivity status. In application to the problem of climate change, it is important to elucidate the role of phytoplankton in the global carbon cycle and workings of marine ecosystems. In this regard, quantitative knowledge, inter alia, on algal cell size distributions in phytoplankton communities permits to assess the rates of carbon deposition to the seabed and, consequently the efficiency of the carbon pump mechanism regulating the carbon fluxes exchange between the atmosphere and ocean [Eppley, Peterson, 1979; Liu et al., 2009; Shovonlal et al., 2013; IOCCG..., 2014].

As the world's largest marginal marine environment, the SCS (Fig. 1) substantially determines the regional climate including its carbon balance aspect [Wong et al., 2007]. At least beyond the coastal zone, this sea is an oligotrophic water body exposed to multiple external forcings including monsoonal seasonal variations in wind conditions, typhoon/tropical-cyclone Wind Pump (WP) [Li, Tang, 2022] and the Kuroshio water intrusions [Nan et al., 2015]. The typhoon WP may cause strong algal blooms even in strictly oligotrophic parts of the SCS, where such intensive blooms would not be possible otherwise.

Here we report on our study addressing such algal blooms in the SCS as local events that appear in both high primary productivity spates and alterations in the phytoplankton community structure (PCS).

Picophytoplankton is known as the most abundant algae in oligotrophic waters, but their abundance and cell size structure prove to be sensitive to changes in the phytoplankton community composition and density, which happens due to the impact of the typhoon WP.

Numerous in situ/ship-borne studies addressed the issue of phytoplankton composition [Pan et al., 2006; Liu et al., 2007; Chen et al., 2009; Huang et al., 2010; Li et al., 2010; Lin et al., 2011; Zhang et al., 2013; Wang et al., 2016]. However, only a few investigations of this subject were based on satellite ocean color remote sensing [Pan et al., 2013; Ye, Tang, 2013; Morozov, Tang, 2019]. The in situ data available to us was used to develop the two algorithms used in the present study [Ye, Tang, 2013; Morozov, Tang, 2019].

The present research is focused on spatio-temporal variations of chl-a depending on the phytoplankton community composition in the SCS within the framework of the typhoon WP phenomenon. We employed two ocean color data processing algorithms for retrieving (a) phytoplankton cell size structure [Ye, Tang, 2013] and (b) *pico*phytoplankton community structure [Morozov, Tang, 2019]. A combination of these two algorithms provided detailed insights into the PCS specific features and dynamics.

Another specific aspect of our study is that it addresses both inter- and intra-annual PCS dynamics. The inter-annual scale is intended to relate the PCS variations to some climatological parameters such as the sea surface temperature (SST), El Nino index and intensity of the Kuroshio intrusion into the SCS. The recent studies show that typhoon WPs significantly affect the marine ecosystem and induce phytoplankton blooms [Zheng, Tang, 2007; Liu et al., 2019; Xu et al., 2019].

On the intra-annual scale, we study the effect of typhoon WPs on the PCS. Previously, there have been no PCS dynamics studies done solely by means of space-borne remote sensing.

The long-term/interannual PCS variability and the factors driving it have not been well studied either. In the present paper we address both of the above issues to reveal how episodic but very intensive/powerful interventions of typhoons affected the PCS against the background of multidecadal PCS variations in the SCS.

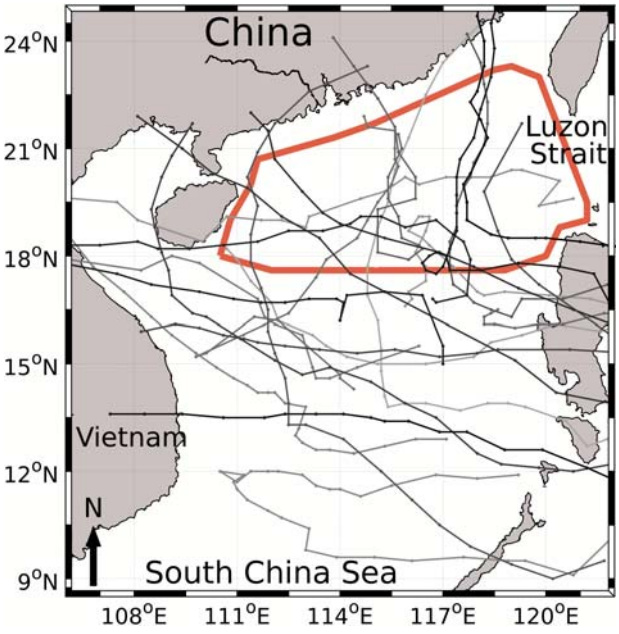

Fig. 1. Study areas in the SCS. Footprints paths of the typhoons that caused algal blooms are shown in various shades of gray. The area in the SCS within which long-term studies were performed is marked as a polygon bounded by a red line

Data sources and research methodology

Data sources

The present study is based on the merged satellite data provided by the Ocean Colour Climate Change Initiative (OC-CCI) Project [2016]. The employed OC-CCI dataset comprises level 3 images at a 4×4 km spatial resolution.

The OC-CCI dataset consolidates radiometrically and spectrally harmonized results from the level 1b, 3rd reprocessing MERIS (MEdium Resolution Imaging Spectrometer) Reduced-Resolution (1 km) data, MODIS level 1A data, R2014.0.1, level 2 VIIRS data, and level 2 Local Area Coverage (1 km) and Global Area Coverage (4 km) SeaWiFS data, R2014.0 [Lee et al., 2002; Mélin, Sclep, 2015; Grant et al., 2017]. The OC-CCI data on remote sensing reflectance R_{rs} are recalculated to match the SeaWiFS spectral bands centered at 412, 443, 490, 510, 555, and 670 nm [Grant et al., 2017]. Monthly and 8-day averaged images were used.

Additionally to OC-CCI data, satellite data on wind and sea surface temperature (SST) were used. Available at www.remss.com [Ricciardulli et al., 2011; Ricciardulli, Wentz, 2016], monthly and weekly averaged wind data are from the Advanced Scatterometer (ASCAT) launched on the EUMETSAT MetOp-A satellite and the Quick Scatterometer (Quikscat). Both the ASCAT and QuikScat data were used at monthly and weekly averaged temporal resolution in bitmap format.

MODIS Level-3 nighttime SST Standard mapped image (SMI) products were utilized [NASA..., 2010]. The product is the skin sea surface temperature in degrees Celsius retrieved from the 11μm and 12 μm spectral channels. The algorithm is based on a modified version of the nonlinear SST algorithm of Walton [Walton et al., 1998; Brown, Minnett, 1999; Kilpatrick et al., 2015]. Available at https://oceancolor.gsfc.nasa.gov, the MODIS-Aqua and MODIS-Terra data cover the entire operational time period extending, respectively, from 04 July 2002 and 24 February 2000 to present [NASA..., 2014]. The MODIS-Terra data were employed only for the time periods of gaps in the MODIS Aqua data availability.

Phytoplankton community structure algorithms

Within the PCS issue, we examined both the proportions of co-existing algal cell size classes and the species composition of the picophytoplankton size class. Two independent satellite OC data processing algorithms were used. One of them, employing a cell size class model, quantifies the percentage of chl-a contained in each of the following three cell size classes: micro-, nano-, and picophytoplankton. The second algorithm determines the cell abundance (cells/ml) in the picophytoplankton class, specifically in the aforementioned *Pro*, *Syn*, and *Peuk* species.

Algorithm for discrimination between algal cell size classes. A Three-Component Model by Ye and Tang (TCM-YT) [Ye, Tang, 2013] for phytoplankton size class analysis in application to the SCS stems from the Brewin et al. [2011] model permitting to ascribe the total chl-a (chl-a_{tot}) in water to three components of phytoplankton, viz. pico-, nano-, and microplankton. To derive the linear relationships between chl-a_{tot} and the above cell-size classes, the TCM-YT employed *in situ* measurements obtained in both open sea and coastal areas of the SCS during different seasons; part of these data were used for the model validation. The resultant linear relationship is further used to re-estimate the distribution of chl-a_{tot} between

the three size classes in order to calculate the micro-, nano-, and picophytoplankton proportions.

The TCM-YT algorithm proved to assure higher correlations and smaller errors as compared with other models when applied to the SCS. The statistical analysis shows that the Root Mean Square Errors (RMSEs) of pico-, nano- and microplankton were 17.6, 9.9 and 9.8 % of chl-a_{tot}, respectively. The TCM-YT performs well with OC-CCI input data from entire SCS, i. e. the marginal and pelagic waters [Ye, Tang, 2013].

Picophytoplankton community structure algorithm. The M&T algorithm by Morozov and Tang [2019] developed for the retrieval of cell concentrations (cell/ml) of three picophytoplankton types, namely the prokaryotic *Prochlorococcus* (*Pro*) and *Synechococcus* (*Syn*), and picoeukaryotes (*Peuk*), in the surface waters of SCS from ocean color satellite data was employed.

The incentive of choosing *Pro*, *Syn* and *Peuk* as the object of our research resides in the invariable interest of marine algologists specifically to these particular picoalgae [Chen et al., 2007, 2009, 2011; Zhang et al., 2013; Wang et al., 2016; Li et al., 2017].

The M&T algorithm is based on the spectral-response approach, exploiting the differences in the optical properties of specific algal groups even if they belong to one and the same cell-size type of phytoplankton. Indeed, it is known that the above three picoalgae have a distinctly specific pigment package composition. As a result, they differ in light harvesting. Besides, their nutrition preferences are different. These dissimilitudes provide additional opportunities to identify each of them. So, the M&T performance can be substantiated by a number of predictors such as reflectance at the wavelengths of satellite sensor's channels, normalized reflectance, log-transformed normalized reflectance, band-ratios and log-transformed band-ratios, and chl-a. Level-3 merged multi-sensor Ocean Colour Climate Change Initiative satellite data were utilized for algorithm development/training. Training was performed with *in situ* data on abundances of the three picophytoplankton groups. Assessed against the training dataset and characterized via the coefficient of correlation (*r*) and the mean absolute percent difference (MAPD), the accuracy of retrieval of algal cell concentrations with the M&T algorithm proved to be 0.90, 0.75, and 0.74 and 34, 59, and 46 % for *Peuk*, *Pro*, and *Syn*, respectively. The regression form that assures the highest accuracy of the algorithm was chosen based on independent data cross-validation (CV). According to the CV independent data tests, the algorithm performance is characterized by *r* and MAPD values of 0.89, 0.72, and 0.73 and 38, 71 and 51 % for *Peuk*, *Pro*, and *Syn*, respectively [Morozov, Tang, 2019].

Data processing

Long-term data series. Monthly mean level-3 OC images were processed with the TCM-YT and M&T algorithms to retrieve the phytoplankton size structure and determine specifically the composition of the picophytoplankton size class. Applying a spatial averaging procedure (to the area marked by the red polygon in Figure 1), spatio-temporal monthly time series were obtained to compute the average annual values of the contribution (%) of micro-, nano-, and picophytoplankton to total chl-a, and the concentrations (cells/ml) of *Pro*, *Syn*, and *Peuk*. The SST and wind data were averaged similarly. The Chl-a data were taken as monthly mean images provided by the OC-CCI Project.

Typhoon events time scale. Monthly and 8-day averaged SST and OC images were taken to study PCS spatial and temporal variations associated with the algal blooms induced by the typhoon WP. The retrieved data were spatially averaged over the typhoon bloom area, which was identified by visual analysis of monthly images. Algal blooms that were apparent in the monthly image were checked for the presence of the typhoon that could have caused them. Figure 2 exemplifies outlining of a typhoon-induced algal bloom area: because the shape of the detected bloom proved to be expressly non-uniform, it was outlined as two separate areas.

As the bloom discernibility in a chl-a image may depend on the background concentrations, and thus no strict thresholds for the algal bloom selection and delineation could be confidently set, the following criteria for the algal bloom identification were employed:

– the bloom is clearly visible in the monthly average chl-a image;

– the bloom or any similar high chl-a feature (area) is not present in the same place in the monthly average image for the previous or subsequent month;

– the onset of the bloom can be tracked down to a typhoon during the analysis of wind speed weekly images.

Delineation of the algal bloom and bloom mask defining for further spatial averaging was done in monthly images. The onset and development of the phytoplankton bloom was studied in temporally averaged 8-days images with spatial averaging over the earlier defined bloom mask (see Fig. 3 for example). In total, 15 typhoon-induced algal blooms were identified. The trajectories of these typhoons are marked with gray lines in Figure 1.

The real number of typhoon-induced algal blooms in the SCS could be greater, but sometimes it was difficult to reliably identify the algal bloom and confidently attribute it to any typhoon. In some cases, algal blooms may become indiscernible because of either storm-driven sediment re-suspension, or river runoff enhancement driven by rainfall, or else the bloom associated with the Kuroshio intrusion. Such blooms were not considered as reliably identified.

3. Results and discussion

Interannual variability

In general, the long-term changes in the SCS state were characterized by a rise in both SST (Fig. 4) and chl-a (Fig. 5, a). The coefficients of correlation between the variations of SST and micro-, nano-, and picophytoplankton shares (Nm, Nn, and Np) over the entire period 2003–2016 were 0.75, 0.79, and 0.91, respectively. The observed growth of the above variables followed the increase of the El Nino index during 1998–2016, which is a manifestation of a long-term process that may be of the same nature as the phenomenon observed in connection with the Kuroshio Current. Nan et al. [2013, 2015] showed that the Kuroshio intrusion into the SCS had a weakening trend in the 1990s and 2000s. These two global oceanic hydrodynamic systems largely underlie PCS variations/changes in the SCS.

In turn, the aforementioned rise in chl-a resulted in an increase in the share of the larger (micro- and nano-) algal cell-size fractions and a decrease in the share of picoalgae in the phytoplankton community (see Fig. 5, b). Therefore, the average cell-size fraction of the phytoplankton became larger.

In terms of cell numbers, the contributions of *Peuk* and *Syn* grew while the contribution of *Pro* decreased (Fig. 6).

An increase in SST should generally lead to stronger stratification and, consequently, to less vertical mixing and lower levels of nutrients, i. e. conditions favorable for the growth of *Pro* [Ting et al., 2002; Fang et al., 2015]. This was not however actually observed in this study. Weaker intrusions of the Kuroshio waters, which are more oligotrophic and more expressly *Pro*-dominated as compared to the SCS waters, should basically correlate with higher chl-a and less *Pro* in the SCS [Li et al., 2017]. This was indeed observed in our study.

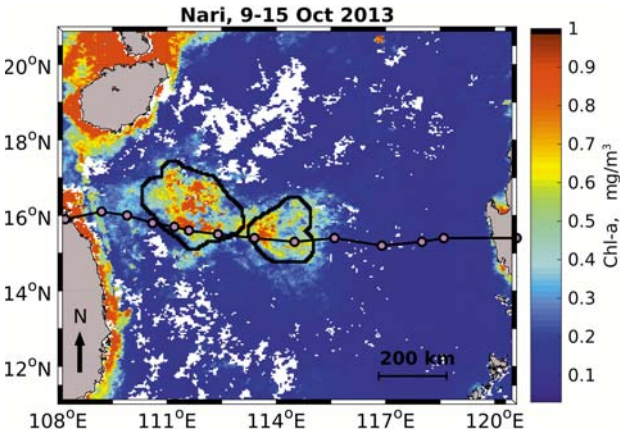

Fig. 2. Typhoon identification example. Black line with pink markers (at three-hour intervals) indicates the path of the typhoon footprint. Black solid line outlines the typhoon-induced bloom

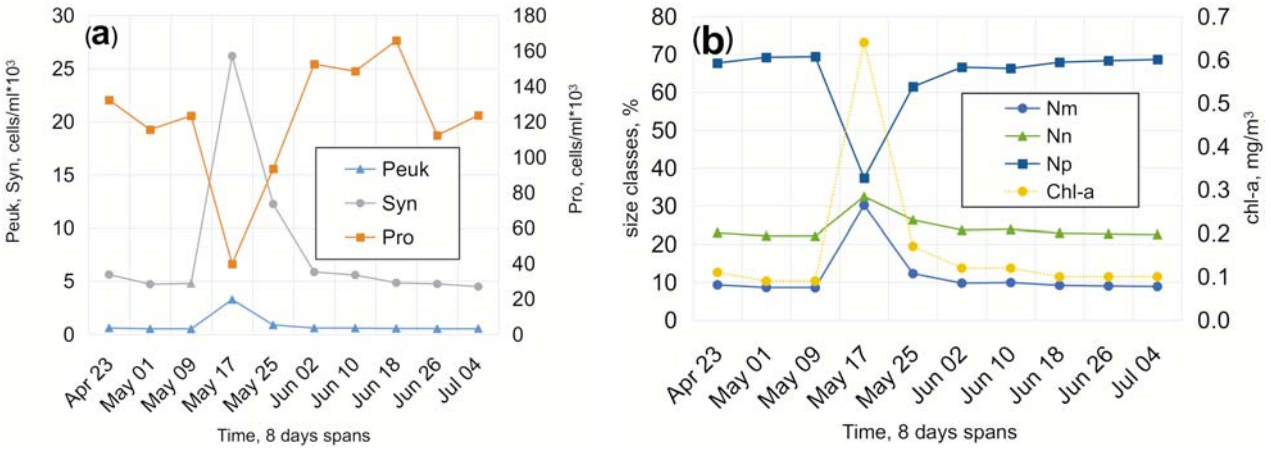

Fig. 3. Example of a weekly (8-day averages) time series of variations in the (a) – *Pro*, *Peuk* and *Syn* cell concentration; (b) – Shares of the micro-, nano- and picophytoplankton in the total chl-a. The data are averaged over the bloom area (the typhoon passage time period is 8–18 May, 2006)

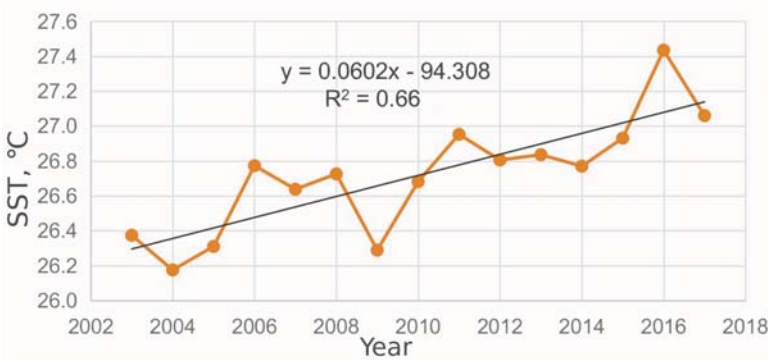

Fig. 4. Variations of the annually averaged SST. Black line is the linear trend

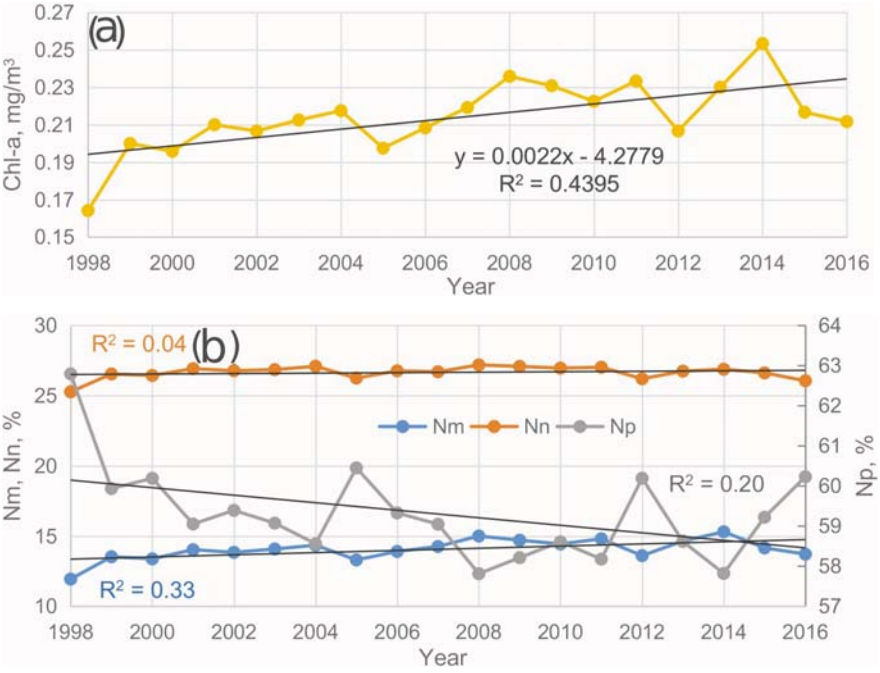

Fig. 5. Interannual variations of (a) – chl-a (yellow line); (b) – blue, orange, and gray lines denote the shares of micro-, nano-, and picophtoplankton in the total chl-a

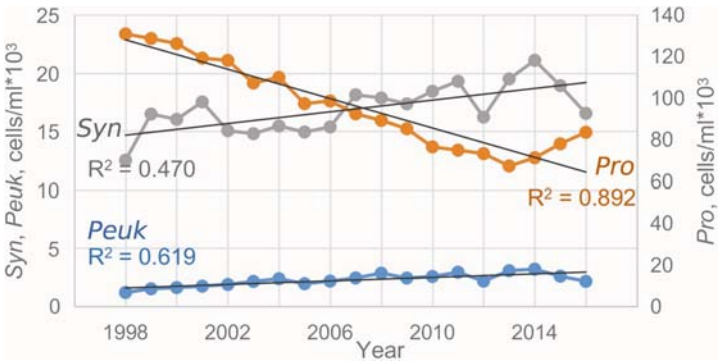

Fig. 6. Interannual variations of *Pro* (orange line), *Syn* (gray line), and *Peuk* (blue line). Black line is the linear trend

The effects produced by El Nino, SST and wind forcing, as well as alterations of the SCS thermohaline structure are arguably main drivers of the PCS long-term changes [Wang et al., 2006; Liu et al., 2015]. However, this issue is beyond the scope of our paper since it is predominantly focused on obtaining space-borne data on PCS and their analysis rather than on in-depth study of the phenomenon's forcing factors, which could be the topic for a separate study.

Seasonal variability

The relationship between the cell-size classes/groups of picophytoplankton was found distinctly expressed in the seasonal cycle the same way as in the long-term/interannual variations, viz. increases in chl-a were accompanied by rising shares of the cell-size groups, viz. Nm, Nn, *Syn*, and *Peuk*, and a reduction in *Pro* concentrations (Fig. 7).

Phytoplankton composition studies at the Southeast Asia Time-series Station in 2001–2002 and 2004–2005 [Liu et al., 2007] revealed the main features of PCS seasonal variations, similar to the intraannual variations observed by us in the SCS area. Indeed, chl-a surface concentrations showed a distinct peak in winter months: as the SST decreases, the MLD deepens and the associated increase in the supply of nutrients follows the intensification of wind mixing. Such winter-time conditions are favorable for most types of phytoplankton with the exception of *Pro*. *Pro* is resistant to low concentrations of nutrients and rather stable light conditions that are generally typical of low MLD [Ting et al., 2002; Moore et al., 1995; Bricaud et al., 1999; Lindell and Post, 1995]. This is illustrated in Figure 7 (d, e, f): *Pro* outnumbered *Syn* and *Peuk* by one and two orders of magnitude, respectively.

Pro did not follow the common seasonal pattern of variations, and being the most abundant picophytoplankton in the area it lowered the relative contribution of picophytoplankton chl-a to the total chl-a. It is noteworthy that although the value of Np is minimal in winter and maximal in summer, the absolute chl-a values of picophytoplankton were higher in winter. The absolute chl-a values are calculated in the following way: $chl\text{-}a_x = chl\text{-}a * N_x$, where the subscript x denotes the phytoplankton cell-size class (m, n, and p for micro-, nano-, and pico-, respectively); $chl\text{-}a_x$ is the chl-a attributed to the cell-size class x; Nx is the contribution/share of algae of cell-size class x to the total chl-a.

Seasonal PCS variations were to a large extent correlated with the seasonal variations of chl-a. The contributions of cell-size classes to $chl\text{-}a_{tot}$

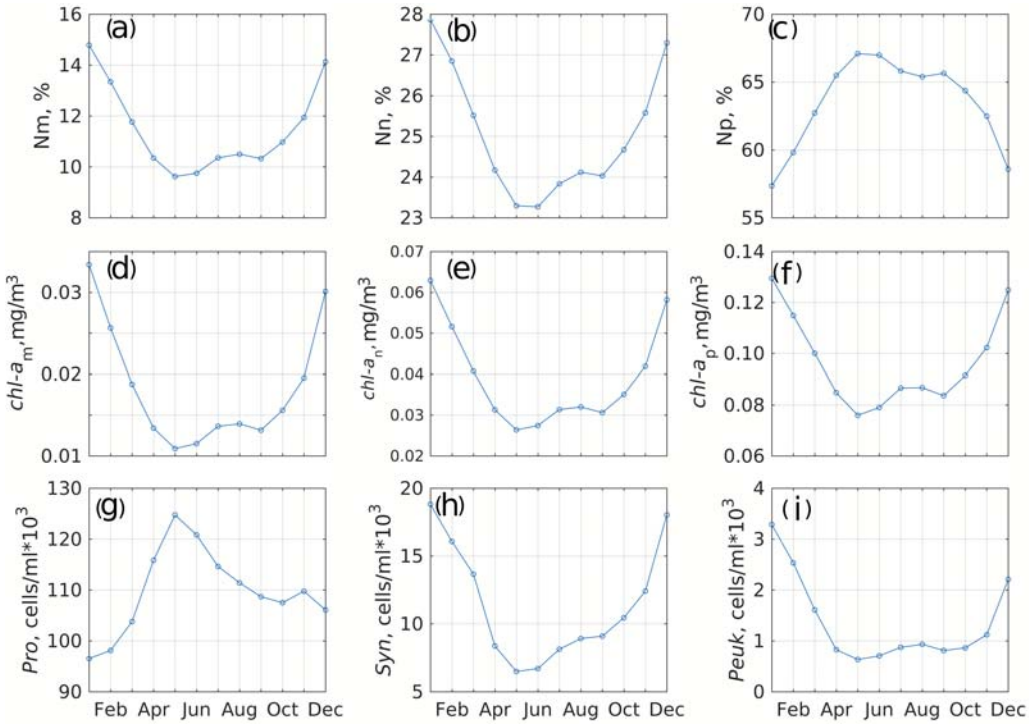

Fig. 7. Mean seasonal variations: shares of the phytoplankton cell size classes: (a) – micro-; (b) – nano-, and (c) – picophytoplankton in the total chl-a; seasonally averaged chl-a concentrations of the three cell-size classes: (d) – micro-; (e) – nano-, and (f) – picophytoplankton; cell concentrations of (g) – *Pro*, (h) – *Syn*, and (i) – *Peuk*

in our research were quantified with the TCM-YT abundance-based algorithm [Ye, Tang, 2013] and are illustrated in Figure 7 (a–c). The contributions of different picophytoplankton cell-size classes to chl-a_{tot} proved to be varying over the year. Nm and Nn were maximal in winter and minimal in summer with the difference between the lowest and highest values of about 5 % of chl-a_{tot} for both cell-size classes (Fig. 7, a, b). The Np was minimal (57 %) in winter and maximal (67 %) in summer, i. e. the difference amounted to 10 %. Although picophytoplankton became a less important contributor to chl-a_{tot} in winter, it remained the most important among the three size classes.

The patterns of seasonal variations in absolute values of chl-a concentrations contributed by each cell-size class were very similar, exhibiting one maximum in winter and two minima in May and September (Fig. 7, d–f). The chl-a of picophytoplankton varied within the range of 0.07–0.13 mg/m^3 and constituted the main portion of the entire chl-a produced in the SCS over the year.

In the annual pattern of *Pro* cell concentrations there were maxima in May and November and one minimum in January (see Fig. 7, g).

Seasonal variations in *Syn* cell concentrations exhibited one maximum in January (or rather in December-January because the maxima were nearly equal in both months) and a minimum in May, followed by a slight decline in September (Fig. 7, h).

Monthly variations in *Peuk* cell concentrations had one maximum in January and two minima occurring in May and September (Fig. 7, i).

Typhoon wind pump-induced variability

All cases. In the above sections we presented and discussed the long-term and large-scale variations in phytoplankton cell-size structure as well as the typical seasonal variations in light of the main oceanographic processes that can initiate/underlie them. This section addresses the PCS changes following the passage of typhoons that induce phytoplankton blooms.

Table 1 presents all the identified typhoon-induced blooms considered in this study. The following designations were used: *Unclear* = bloom is relatively weak and its area is difficult to delineate; *Clear* = bloom boundaries are well expressed; *Intrusion* = bloom may have been affected by the Kuroshio intrusion into the SCS; *Coastal* = bloom was caused by a typhoon WP but was likely affected by coastal runoff or near-shore sediment re-suspension. Typhoon Maria (typhoon #2) was considered together with typhoon Wukong because the bloom was mostly caused by typhoon Maria: Wukong travelled closely

Table 1. The list of typhoon WP-caused blooms and the associated information

No	Name	Typhoon dates	Bloom dates	Bloom type	Bloom duration, weeks	coast	intru-sion	Bloom area, km^2	Max Chl-a 8d mean
1	Leo	27 Apr – 2 May 1999	1–16 May	Unclear	2	–	–	27,744	0.85
2	Maria (+Wukong)	28 Aug – 1 Sept 2000 5–10 Sept 2000	5–12 Sept	Unclear	1	–	–	10,832	0.25
3	Lingling	6–12 Nov 2001	11 Nov – 2 Dec	Open sea, clear, very large	3-4	–	–	89,680	0.49
4	Nepartak	13–19 Nov 2003	17 Nov – 2 Dec	Open sea, clear, weak	1-2	–	–	24,704	0.27
5	Nanmadol	28 Nov – 3 Dec 2004	24 Nov – 25 Dec	Intrusion	3-4	+	+	12,384	0.70
6	Damrey (#17)	21–27 Sept 2005	22 Sep – 7 Oct	Coastal	2	+	–	13,584	0.69
7	Kai-Tak (#22)	8 Oct – 2 Nov 2005	1–4 Nov	Open sea, clear	2-3	–	–	11,424	2.07
8	Changchu	8–18 May 2006	17 May – 1 Jun	Open sea, clear visible	1-2	–	–	48,128	0.64
9	Cimaron	27 Oct – 4 Nov 2006	1–24 Nov	Open sea, visible	2-3	–	–	12,288	0.24
10	Lekima	30 Sept – 3 Oct 2007	8 Oct – 8 Nov	Coastal	2	+	–	19,472	0.79
11	Hagibis	19–27 Nov 2007	25 Nov – 26 Dec	Open sea, visible	3-4	–	–	62,304	1.66
12	Typhoon #2	13–19 Apr 2008	14–21 April	Open sea, weak	1	+	–	73,360	0.22
13	Linfa (#3)	13–22 Jun 2009	18 Jun – 11 Jul	Open sea, clear	2-3	–	–	7,344	0.41
14	Megi	13–23 Oct 2010	24 Oct – 24 Nov	open sea, intrusion	3-4	–	–	19,216	1.41
15	Jebi	8–14 Aug 2013	28 Jul – 12 Aug	Open sea, weak	1-2	–	–	15,696	0.21
16	Nari	9–15 Oct 2013	16 Oct – 16 Nov	Open sea, clear	3-4	–	–	52,720	0.79
17	Rammasun	12–19 Jul 2014	20–28 Jul	Open sea, weak	1	–	–	61,552	0.17

to the footprint of Maria and therefore it was difficult to separate the influence of one from the other.

Since some of the bloom cases listed in Table 1 were studied by others, it was possible to obtain additional information on the conditions of bloom initiation and its development. A summary description of the blooms selected for the present study is given in Table 2, which also contains information on data sources for each bloom, its origin and the mechanism by which the bloom was produced.

Typical bloom development. A typical typhoon-induced bloom is characterized by increased chl-a_{tot} with the prevalent chl-a and cell count contribution to the phytoplankton community from larger (micro- and nano-) algal groups. At the same time, the picophytoplankton contribution decreases. Within the picophytoplankton cell-size class, the changes are multidirectional: *Synechococcus* and Picoeukaryotes cell counts increase while that of *Prochlorococcus* declines.

In the case of a typhoon WP event in the open sea, storm wind-induced water mixing and upwelling conjointly lead to an increase in both MLD and the Ekman layer depth, with a result of bringing nutrient-rich deep waters to the surface and stimulating phytoplankton growth [Zhao et al., 2008, 2009; Yang, Tang, 2010; Chen et al., 2011; Chen, Tang, 2012; Yu et al., 2013]. Another important mechanism of phytoplankton concentration increase can reside in the presence of a subsurface maximum, which becomes mixed up with the surface waters due to the typhoon-induced upwelling [Ye et al., 2013, 2018a, b; Xu et al., 2019].

Being resistant to nutrient-poor conditions, the smaller cell-sized (pico-) phytoplankton benefit from this sudden increase in nutrient availability not so much as the larger cell-sized (micro- and nano) phytoplankton. Within the picophytoplankton community, *Syn* and *Peuk* generally benefit from the increased nutrient supply. Contrarily, *Pro*, which prefers oligotrophic stratified waters, is the only phytoplankton group that is depressed by the typhoon. Its share in chl-a_{tot} goes down, while the populations of *Syn* and *Peuk* are enlarged.

Because of its specific light harvesting system, *Pro* prefers growing at some depth [Ting et al., 2002]. Thus, an alternative or additional mechanism of downgrading the status of *Pro* in the phytoplankton community might be a sudden lifting of *Pro* cells closer to the surface due to typhoon-driven water pumping with the eventual effect of reducing the growth of these algae. While, e.g., *Syn* algae are generally distributed rather uniformly in the upper part of the euphotic zone (0–50 m), the water pumping effect alone, in the absence of nutrient enrichment, would not affect the abundance of this species [Li et al., 2017].

In some cases, the typhoon-related forcings may also include heavy rainfall resulting in intensification of river/land runoff [Zheng et al., 2007]. The Kuroshio intrusion is another possible factor capable of affecting the PCS in the SCS, e. g. case #5 [Tang et al., 1999; Li et al., 2017].

Open sea bloom induced by typhoon. One of the examples is the bloom caused by Typhoon Chanchu on 8–18 May 2006 (see Fig. 8). The phases of the onset and unfolding of the bloom were clearly distinguishable and the associated changes in the PCS could be confidently detected, quantified and interpreted. A similar example (typhoon Nari) is illustrated in Figures 2 and 3.

The 8-day-averaged spatio-temporal time series of the PCS changes induced by Typhoon #2 are presented in Figure 8 (b). The bloom lasted

Table 2. Blooms studied and reported elsewhere and the associated information

Case #	Typhoon	Typhoon Date	Reference	Bloom formation mechanism
3	Lingling	6–12 Nov 2001	Zhao et al., 2008 Yang, Tang, 2010	Strong, fast-moving typhoon
5	Nanmadol	28 Nov – 3 Dec 2004	Tang et al., 1999 (similar case)	Winter-time upwelling in Luzon Strait
6	Damrey	21–27 Sept 2005	Zheng, Tang, 2007 Zhao et al., 2009 (similar case)	Coastal runoff due to typhoon associated rainfall
7	Kai-Tak	8 Oct – 2 Nov 2005	Zhao et al., 2008 Yu et al., 2014 Yang, Tang, 2010	Weak, slow-moving typhoon
11	Hagibis	19–27 Nov 2007	Sun et al., 2010	Long forcing time, strong upwelling
13	Linfa	13–22 Jun 2009	Chen, Tang, 2012 Liu et al., 2019	Multiple passage of 1 typhoon
16	Wutip Nari	26–30 Sept 2013 9–15 Oct 2013	Ye et al., 2017	Wind mixing and upwelling

Note. Water vertical mixing and upwelling were possibly the accompanying processes in all cases of the listed typhoons.

for 2 weeks (May 17 – May 25 in Figure 8, b), and during this time period clouds did not interfere with the observations so that the data coverage was not less than 94 % (see Fig. 8, b). Data coverage is the percent of the 8-day average image covered by cloud free satellite data. The bloom started intensively in the first 8 days right after the typhoon had passed (May 18 in Fig. 8, b). The bloom exhibited all the typical features specified in section 3.3.2. In the second week (May 25 in Fig. 8, b), the bloom-induced changes in the PCS remained clearly discernible: *Pro* and *Syn* abundances were still very low and high, respectively. It is also worth noting that during the second week, the bloom was barely noticeable in the spatial distribution of chl-a (Fig. 8, b) but it stayed distinctly expressed in the patterns of the PCS parameters, especially, Nn, Np, *Pro*, and *Syn*.

Coastal zone bloom induced by typhoon. Typhoon Damrey passed the area during two weeks (21 and 27 September 2005 in Fig. 9). The coastal runoff affected the development of the typhoon-induced bloom. Figure 9 illustrates the typhoon footprint trajectory, successive bloom locations (Fig. 9, a) and the associated chl-a dynamics (Fig. 9, b). The co-occurring coastal runoff prolonged the bloom lifetime: the bloom remained very strong during two weeks with the maximum in the second week [Zheng, Tang, 2007].

Combined effect of typhoon passage and the Kuroshio intrusion. The decrease in the picophytoplankton cell numbers produced by Nanmadol typhoon (28 Nov – 3 Dec 2004) proved to be not so strong as in the two previously discussed cases (Fig. 10, a). This may be due to the intrusion of highly oligotrophic and *Pro*-rich Kuroshio waters [Li et al., 2017]. Remarkably, the most prominent bloom feature appeared in the chl-a spatial distribution prior to the actual passage of the typhoon (Fig. 10, b). So, it would be more appropriate to speak of a contribution of the invading typhoon to the already existing bloom rather than of the bloom actually triggered by the typhoon.

Typhoon-induced blooms discussed in this study can be roughly classified into three types, i.e. open-sea bloom induced by typhoon, bloom induced by typhoon with the “assistance” of coastal water nutrients, and bloom induced by typhoon with the “assistance” of the Kuroshio.

Such a classification is certainly rather speculative since in the absence of matchup oceanographical data, it is hardly possible to ascertain the nature of the processes involved in the formation of a concrete bloom. In real life, the bloom initiation is prompted either by one of such factors as proximity to the coast (for instance, in the Luzon Strait area), the Kuroshio intrusion, wintertime Luzon Strait upwelling, or even by a combination of the said factors. Further extension of the number of studied/analyzed typhoon-related cases may be helpful in understanding the mechanisms that determine the PCS dynamics in the SCS.

Conclusions

Application of the TCM-YT and M&T retrieval algorithms to the OC CCI data permitted investigating the PCS variations in the SCS on different time scales.

Long-term (1998–2016) PCS changes followed the rise in chl-a levels that continued throughout this period and were marked by a redistribution of the shares of micro-, nano- and picophytoplankton groups in favor of the algae with a larger cell size.

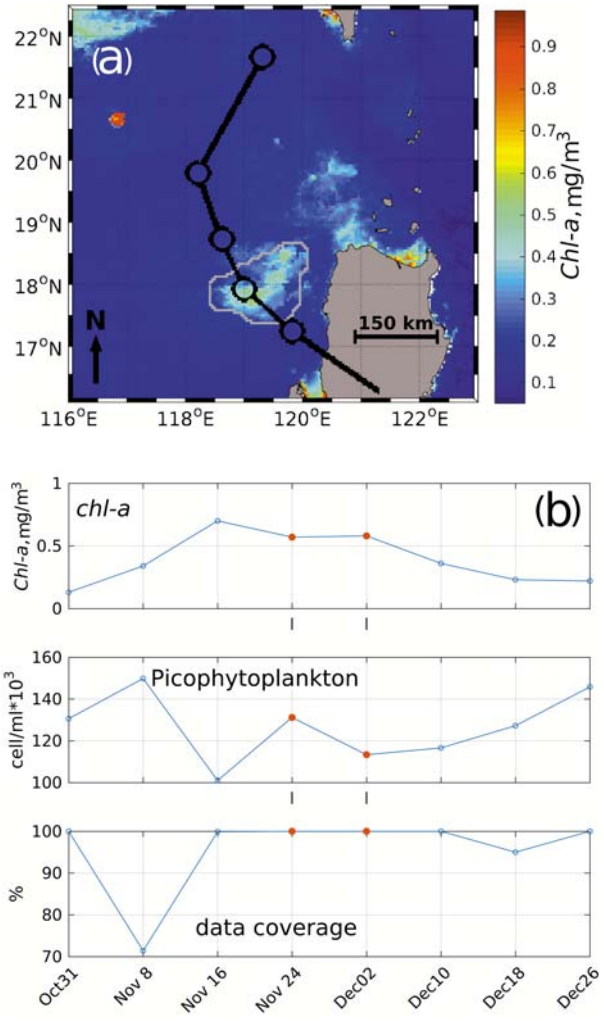

Fig. 8. Outlined area of the bloom caused by the Chanchu typhoon (8–18 May 2006) in the oligotrophic open sea region (a); 8-day spatio-temporal time series averaged over the typhoon-induced bloom area (b). The red dot is the week of the typhoon event

Within the picophytoplankton group, the concentration of *Pro*, the smallest cell-size species, decreased while the abundance of *Syn* and *Peuk* species remained largely unaltered.

During the long-term period, similar patterns were found in the PCS *seasonal* variations, which indicates that the entire PCS variability was primary due to the *Pro* algae.

Investigation of blooms initiated by typhoon WP showed that an increase in chl-a was invariably accompanied by an increase of the micro- and nanophytoplankton share in chl-a_{tot}, while picophytoplankton's share clearly tended downward. The same applies to the respective cell numbers.

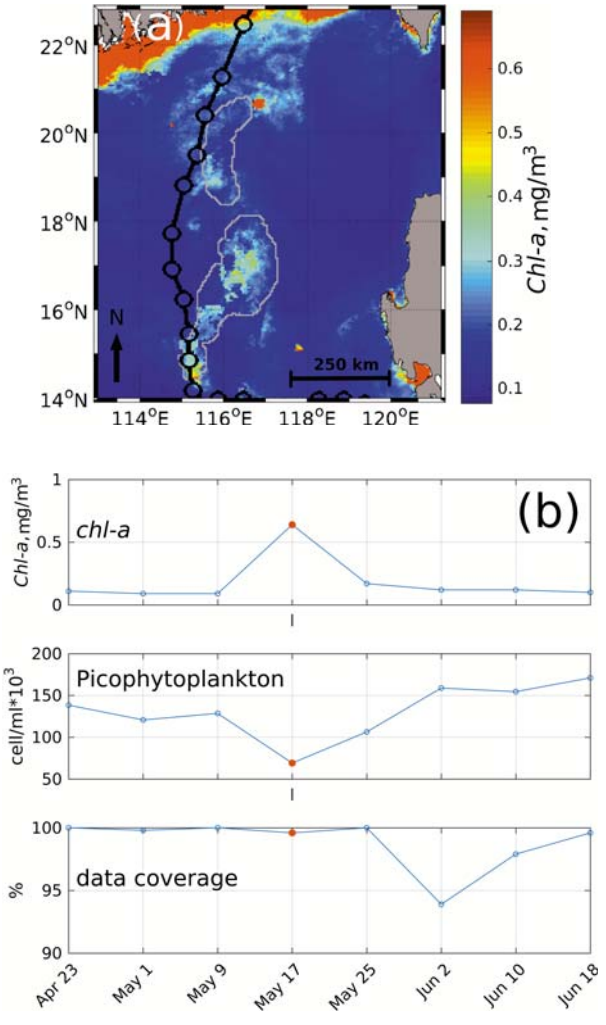

Fig. 9. Outlined areas of the bloom caused by the Damrey typhoon, which occurred in the context of enhanced land runoff and possibly bottom sediment re-suspension (a); 8-day spatio-temporal time series averaged over the typhoon-induced bloom area (b); the red dot is the week of the typhoon event

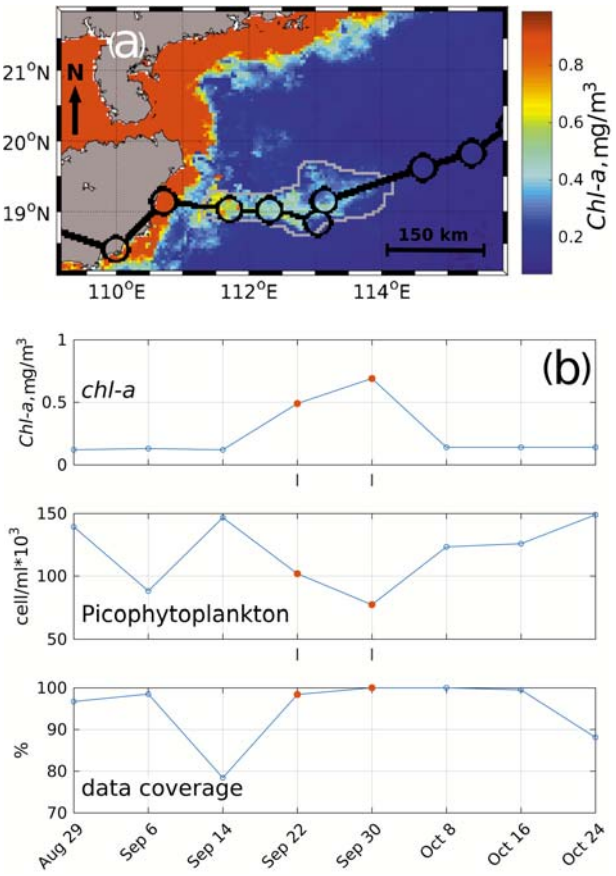

Fig. 10. Outlined areas of the bloom caused by the Nanmadol typhoon in combination with the Kuroshio intrusion (a); 8-day spatio-temporal time series averaged over the typhoon-induced bloom area (b)

It was found that the typhoon WP impact upon the PCS in the SCS extends over an area of about 100–300 km, and can last up to 4 weeks, but usually its lifetime is 2 weeks.

The results indicate that the above two data processing algorithms are instrumental in establishing the PCS status and its dynamics in the SCS, especially when respective ship-borne data with appropriate spatial coverage and time-and space resolution are unavailable.

Nevertheless, it should be noted that the intensity and spatial extent of the typhoon-driven impacts on the PCS can be fashioned by the presence of a bloom formed prior to the typhoon arrival, as well as by lifting of deep-water nutrients closer to the surface. The Kuroshio invasion, proximity to the coast or the wintertime Luzon Strait permanent upwelling can arguably augment/modulate the actual influence of the typhoon WP on the PCS in the SCS. These are the aspects of the typhoon WP phenomenon calling for further investigation.

References

Bai Y., He X., Yu S., Chen C.-T. A. Changes in the ecological environment of the marginal seas along the Eurasian continent from 2003 to 2014. *Sustainability*. 2018;10:635. doi: 10.3390/su10030635

Brewin R. J. W., Hardman-Mountford N. J., Lavender S. J., Raitsos D. E., Hirata T., Uitz J., Devred E., Bricaud A., Ciotti A., Gentili B. An intercomparison of bio-optical techniques for detecting dominant phytoplankton size class from satellite remote sensing. *Remote Sensing Environ.* 2011;115:325–339. doi: 10.1016/j.rse.2010.09.004

Bricaud A., Allali K., Morell A., Marie D., Veldhuis M. J. W., Partensky F., Vaulot D. Divinyl chlorophyll a-specific absorption coefficients and absorption efficiency factors for Prochlorococcus marinus: kinetics of photoacclimation. *Mar. Ecol. Prog. Ser.* 1999;188: 21–32. doi: 10.3354/meps188021

Brown O. B., Minnett P. J. MODIS infrared sea surface temperature algorithm — Algorithm Theoretical Basis Document (technical report, product MOD28). University of Miami. Miami; 1999. 83 p.

Chen Y.-L. L., Chen H.-Y., Lin I.-I., Lee M.-A., Chang J. Effects of cold eddy on phytoplankton production and assemblages in Luzon Strait bordering the South China Sea. *J. Oceanogr.* 2007;63:671–683. doi: 10.1007/s10872-007-0059-9

Chen B., Liu H., Landry M. R., Dai M., Huang B., Sun J. Close coupling between phytoplankton growth and microzooplankton grazing in the western South China Sea. *Limnol. Oceanogr.* 2009;54(4):1084–1097. doi: 10.4319/lo.2009.54.4.1084

Chen X., Pan D., He X., Bai Y., Wang D. Phytoplankton bloom and sea surface cooling induced by Category 5 Typhoon Megi in the South China Sea: direct multi-satellite observations. *Proc. SPIE 8175, Remote Sensing of the Ocean, Sea Ice, Coastal Waters, and Large Water Regions*. 2011;817519. doi: 10.1117/12.897853

Chen Y., Tang D. Eddy-feature phytoplankton bloom induced by a tropical cyclone in the South China Sea. *Int. J. Remote Sens.* 2012;33(23):7444–7457. doi: 10.1080/01431161.2012.685976

Eppley R. W., Peterson B. J. Particulate organic matter flux and planktonic new production in the deep ocean. *Nature*. 1979;282:677–680.

Fang M., Ju W., Liu X., Yu Z., Qiu F. Surface chlorophyll-a concentration spatio-temporal variations in the northern South China Sea detected using MODIS data. *Terr. Atmos. Ocean. Sci.* 2015;26(3):319–329. doi: 10.3319/TAO.2014.11.14.01(Oc)

Grant M., Jackson T., Chuprin A., Sathyendranath S., Zühlke M., Dingle J., Storm T., Boettcher M., Fomferra N. Ocean Colour Climate Change Initiative (OC_CCI) – Phase two, Product user guide / Plymouth Marine Laboratory. 2017. Iss. 3.1.0.

Huang B., Hu J., Xu H., Cao Z., Wang D. Phytoplankton community at warm eddies in the northern South China Sea in winter 2003/2004. *Deep Sea Res. II: Topical Studies in Oceanography*. 2010;57(19–20): 1792–1798. doi: 10.1016/j.dsr2.2010.04.005

IOCCG. Phytoplankton functional types from space. Sathyendranath S. (ed.). Reports of the International ocean-colour coordinating group No. 15, Dartmouth, Canada; 2014. 154 p. doi: 10.25607/OBP-106

Kilpatrick K. A., Podestá G., Walsh S., Williams E., Halliwell V., Szczodrak M., Brown O. B., Minnett P. J., Evans R. A decade of sea surface temperature from MODIS. *Remote Sens. Environ*. 2015;165:27–41. doi: 10.1016/j.rse.2015.04.023

Lee Z. P., Carder K. L., Arnone R. Deriving inherent optical properties from water color: A multi-band quasi-analytical algorithm for optically deep waters. *Appl. Opt.* 2002;41:5755–5772. doi: 10.1364/AO.41.005755

Lindell D., Post A. F. Ultraplankton succession is triggered by deep winter mixing in the Gulf of Aqaba (Eilat) Red Sea. *Limnol. Oceanogr.* 1995;40:1130–1141. doi: 10.4319/lo.1995.40.6.1130

Lin Q., Yin J., Huang L., Li K., Xiong L. Phytoplankton community structure in waters of continental shelf in the northwestern South China Sea in spring 2007. *J. Oceanogr. Taiwan Strait.* 2011;30(4):559–569.

Li T., Liu S., Wang G., Cao W., Huang L., Lin Q. Species composition of phytoplankton and its distribution in the northern South China Sea in autumn. *J. Tropic. Oceanogr*. 2010;29(2):65–73.

Li J., Jiang X., Li G., Jing Z., Zhou L., Ke Z., Tan Y. Distribution of picophytoplankton in the northeastern South China Sea with special reference to the effects of the Kuroshio intrusion and the associated mesoscale eddies. *Sci. Total Environ.* 2017;589:1–10. doi: 10.1016/j.scitotenv.2017.02.208

Li Y., Tang D. Tropical cyclone Wind Pump induced chlorophyll-a enhancement in the South China Sea: A comparison of the open sea and continental shelf. *Front. Mar. Sci.* 2022;9:1039824. doi: 10.3389/fmars.2022.1039824

Liu H., Chang J., Tseng C.-M., Wen L.-S., Liu K. K. Seasonal variability of picophytoplankton in the Northern South China Sea at the SEATS station. *Deep Sea Res. II.* 2007;54:1602–1616. doi: 10.1016/j.dsr2.2007.05.004

Liu H., Chang J., Tseng C.-M., Wen L.-S., Liu K. K. Seasonal variability of picophytoplankton in the Northern South China Sea at the SEATS station. *Deep Sea Res. II.* 2007;54:1602–1616. doi: 10.1016/j.dsr2.2007.05.004

Liu M., Liu X., Ma A., Zhang B., Jing M. Spatio-temporal variability of chlorophyll-a and sea surface temperature in the northern South China Sea from 2002 to 2012. *Can. J. Remote Sens*. 2015;41(6):547–560. doi: 10.1080/07038992.2015.1112728

Liu H., Probert I., Uitz J., Claustre H., Aris-Brosou S., Frada M., Not F., de Vargas C. Extreme diversity in noncalcifying haptophytes explains a major pigment paradox in open oceans. *Proceedings of the National Academy of Sciences*. 2009;106(31):12803–12808. doi: 10.1073/pnas.0905841106

Liu Y., Tang D., Morozov E. Chlorophyll concentration response to the typhoon Wind-Pump induced upper ocean processes considering air-sea heat exchange. *Remote Sens.* 2019;11(15):1825. doi: 10.3390/rs11151825

Mélin F., Sclep G. Band shifting for ocean color multi-spectral reflectance data. *Optics Express.* 2015;23:2262–2279. doi: 10.1364/OE.23.002262

Moore R. L., Goericke R., Chisholm W. S. Comparative physiology of *Synechococcus* and *Prochloro-*

coccus: influence of light and temperature on growth, pigments, fluorescence and absorptive properties. *Mar. Ecol. Progr. Ser.* 1995;116:259–275. doi: 10.3354/meps116259

Morozov E., Tang D. Satellite ocean colour algorithm for Prochlorococcus, Synechococcus, and picoeukaryotes concentration retrieval in the South China Sea. *Adv. Space Res.* 2019;63:16–31. doi: 10.1016/j.asr.2018.07.005

Nan F., Xue H., Chai F., Wang D., Yu F., Shi M., Guo P. Weakening of the Kuroshio intrusion into the South China Sea over the past two decades. *J. Clim.* 2013;26:8097–8110. doi: 10.1175/JCLI-D-12-00315.1

Nan F., Xue H., Yu F. Kuroshio intrusion into the South China Sea: A review. *Progr. Oceanogr*. 2015;137:314–333. doi: 10.1016/j.pocean.2014.05.012

NASA Goddard Space Flight Center, Ocean Ecology Laboratory, Ocean Biology Processing Group. 2014. Moderate Resolution Imaging Spectroradiometer (MODIS) SST Data, NASA OB. DAAC. URL: https://oceancolor.gsfc.nasa.gov/cgi/browse.pl?sen=amod (accessed: 15.01.2024).

NASA. Ocean Level-3 Standard Mapped Image Products, June 4. 2010. URL: https://oceancolor.gsfc.nasa.gov/docs/format/Ocean_Level-3_SMI_Products.pdf (accessed: 25.03.2024).

OC-CCI. Ocean Colour Climate Change Initiative dataset, Version 3.1.0, European Space Agency. 2016. URL: https://www.oceancolour.org (accessed: 10.02.2024).

Pan L. A., Zhang J., Chen Q., Deng B. Picophytoplankton community structure at a coastal front region in the northern part of the South China Sea. *J. Plankton Res.* 2006;28(3):337–343. doi: 10.1093/plankt/fbi117

Pan X., Wong G. T. F., Ho T.-Y., Shiah F.-K., Liu H. Remote sensing of picophytoplankton distribution in the northern South China Sea. *Remote Sens. Environ.* 2013;128:162–175. doi: 10.1016/j.rse.2012.10.014

Ricciardulli L., Wentz F. J., Smith D. K. Remote sensing systems QuikSCAT Ku-2011 ocean vector winds on 0.25 deg grid, Version 4. Remote Sensing Systems, Santa Rosa, CA; 2011. URL: https://www.remss.com/missions/qscat (accessed: 10.01.2024).

Ricciardulli L., Wentz F. J. April 2016. Remote sensing systems ASCAT. Daily ocean vector winds on 0.25 deg grid, Version 02.1. Remote Sensing Systems, Santa Rosa, CA; 2015. URL: https://www.remss.com/missions/ascat (accessed: 10.01.2024).

Shovonlal R., Sathyendranath S., Bouman H., Platt T. The global distribution of phytoplankton size spectrum and size classes from their light-absorption spectra derived from satellite data. *Remote Sens. Environ*. 2013;139:185–197. doi: 10.1016/j.rse.2013.08.004

Sun L., Yang Y.-J., Xian T., Lu Z., Fu Y.-F. Strong enhancement of chlorophyll a concentration by a weak typhoon. *Mar. Ecol. Prog. Ser.* 2010;404:39–50. doi: 10.3354/meps08477

Tang D.-L., Ni I.-H., Kester D. R., Muller-Karger F. E. Remote sensing observations of winter phytoplankton blooms southwest of the Luzon Strait in the South China Sea. *Mar. Ecol. Prog. Ser.* 1999;191:43–51. doi: 10.3354/meps191043

Ting C. S., Rocap G., King J., Chisholm S. W. Cyanobacterial photosynthesis in the oceans: the origins and significance of divergent light-harvesting strategies. *Trends Microbiol*. 2002;10(3):134–142. doi: 10.1016/S0966-842X(02)02319-3

Walton C. C., Pichel W. G., Sapper J. F., May D. A. The development and operational application of nonlinear algorithms for the measurement of sea surface temperatures with the NOAA polar-orbiting environmental satellites. *J. Geophys. Res.* 1998;103(C12):27999–28012. doi: 10.1029/98JC02370

Wang J., Tan Y., Huang L., Ke Z., Tan J., Hu Z., Wang Q. Response of picophytoplankton to a warm eddy in the northern South China Sea. *Oceanol. Hydrobiol. Stud.* 2016;45(2):145–158. doi: 10.1515/ohs-2016-0014

Wang C., Wang W., Wang D., Wang Q. Interannual variability of the South China Sea associated with El Niño. *J. Geophys. Res.* 2006;111:C03023. doi: 10.1029/2005JC003333

Wong G. T. F., Ku T. L., Mulholland M., Tseng C. M., Wang. D. P. The South East Asian Time-series Study (SEATS) and the biogeochemistry of the South China Sea – an overview. *Deep Sea Res. II.* 2007;54:1434–1447. doi: 10.1016/j.gca.2012.08.039

Xu H., Tang D., Liu Y., Li Y. Dissolved oxygen responses to tropical cyclones 'Wind Pump' on pre-existing cyclonic and anticyclonic eddies in the Bay of Bengal. *Mar. Pollut. Bull.* 2019;146:838–847. doi: 10.1016/j.marpolbul.2019.07.019

Yang X., Tang D. Location of sea surface temperature cooling induced by typhoon in the South China Sea. *J. Tropic. Oceanogr.* 2010;29(4):26–31. (In Chinese). doi: 10.11978/2016045

Ye H., Kalhoro M. A., Sun J., Tang D. Chlorophyll blooms induced by tropical cyclone Vardah in the Bay of Bengal. *Indian J. Geomarine Sci.* 2018a;47(07):1383–1390.

Ye H., Sheng J., Tang D., Morozov E., Kalhoro A. M., Wang S., Xu H. Examining the impact of tropical cyclones on air-sea CO2 exchanges in the Bay of Bengal based on satellite data and *in situ* observations. *J. Geophys. Res.: Oceans.* 2018b;123:555–576. doi: 10.1029/2018JC014533

Ye H., Sheng J., Tang D., Siswanto E., Kalhoro M. A., Sui Y. Storm-induced changes in pCO2 at the sea surface over the northern South China Sea during Typhoon Wutip. *J. Geophys. Res.: Oceans.* 2017;122:1-18. doi: 10.1002/2016JC012643

Ye H., Sui Y., Tang D., Afanasyev Y. D. A subsurface chlorophyll a bloom induced by typhoon in the South China Sea. *J. Marine Syst.* 2013;128:138–145. doi: 10.1016/j.jmarsys.2013.04.010

Ye H., Tang D. A three-component model of phytoplankton size classes for the South China Sea. *Malays. J. Sci.* SCS Sp Iss. 2013;32:319–326.

Yu J., Tang D., Chen G., Li Y., Huang Z., Wang S. The positive effects of typhoons on the fish CPUE in the South China Sea. *Continental Shelf Res.* 2014;84:1–12. doi: 10.1016/j.csr.2014.04.025

Yu J., Tang D., Li Y., Huang Z., Chen G. Increase in fish abundance during two typhoons in the South China Sea. *Adv. Space Res.* 2013;51:1734–1749. doi: 10.1016/j.asr.2012.11.019

Zhang X., Shi Z., Ye F., Zeng Y., Huang X. Picophytoplankton abundance and distribution in three contrasting periods in the Pearl River Estuary, South China. *Mar. Freshwater Res.* 2013;64:692–705. doi: 10.1071/MF12303

Zhao H., Tang D., Wang Y. Comparison of phytoplankton blooms triggered by two typhoons with different intensities and translation speeds in the South China Sea. *Mar. Ecol. Prog. Ser.* 2008;365:57–65. doi: 10.3354/meps07488

Zhao H., Tang D., Wang D. Phytoplankton blooms near the Pearl River Estuary induced by Typhoon Nuri. *J. Geophys. Res.* 2009;114:C12027. doi: 10.1029/2009JC005384

Zheng G., Tang D. Offshore and nearshore chlorophyll increases induced by typhoon winds and subsequent terrestrial rainwater runoff. *Mar. Ecol. Prog. Ser.* 2007;333:61–74. doi: 10.3354/meps333061

Поступила в редакцию / received: 31.01.2025; принята к публикации / accepted: 04.03.2025.
Авторы заявляют об отсутствии конфликта интересов / The authors declare no conflict of interest.

СВЕДЕНИЯ ОБ АВТОРАХ:

Морозов Евгений Александрович
канд. физ.-мат. наук, старший научный сотрудник Отдела дистанционных методов исследований
e-mail: frisman@list.ru

Йе Хайджун
канд. физ.-мат. наук, доцент
e-mail: yehaijun309@126.com

Тан Данлин
д-р физ.-мат. наук, профессор
e-mail: lingzistdl@126.com

Поздняков Дмитрий Викторович
д-р физ.-мат. наук, профессор, заместитель директора по науке, руководитель группы водных экосистем
e-mail: dmitry.pozdnyakov@niersc.spb.ru

Лиу Ипэн
канд. физ.-мат. наук, ст. преподаватель
e-mail: 457123806@qq.com

CONTRIBUTORS:

Morozov, Evgenii
Cand. Sci. (Phys.-Math.), Senior Researcher

Ye, HaiJun
PhD (Phys.-Math.), Associate Professor

Tang, DanLing
DSc (Phys.-Math.), Full Professor

Pozdnyakov, Dmitry
Dr. Sci. (Phys.-Math.), Full Professor

Liu, YuPeng
PhD (Phys.-Math.), Assistant Professor